Received: 20 February 2019 | Revised: 1 June 2019 | Accepted: 8 July 2019

DOI: 10.1002/2050-7038.12158

RESEARCH ARTICLE

WILEY

Closed-loop control and performance analysis of a high-gain buck-boost converter with optimized Type III controller

Subrata Banerjee | Niraj Rana

Department of Electrical Engineering, National Institute of Technology Durgapur, Durgapur, India

Correspondence
Niraj Rana, Department of Electrical Engineering, National Institute of Technology Durgapur, Durgapur 713209, India.
Email: nirajranaosme@gmail.com

Summary

This paper presents the design and development of an improved high-gain buck-boost converter (HGBBC) with optimized Type III controller suitable for power supplies in various electrical/electronics devices. The proposed HGBBC produces higher efficiency, exhibits better performance, is less bulky, and is compact in size. The voltage gain of the proposed HGBBC is the squared times the voltage gain of the conventional buck-boost converter (BBC). The polarity of source and load (output) voltages are the same (ie, noninverting polarity). This added advantage of the proposed converter allows it to operate the positive load voltage variation in a wider range even with small variation of duty cycle ratio of the power switches. Therefore, its application may be advantageous for electronics/electrical equipment. The proposed converter's validity is determined by its steady-state analysis, small-signal analysis, and closed loop control operation. A closed-loop controlled of HGBBC utilizing optimized Type III controller has been fabricated and tested in the laboratory. The comparative studies in terms of efficiency, dynamic response, and percentage ripple content of the proposed HGBBC and existing converters have been performed. From the results, it is seen that the proposed HGBBC is performed better than other existing quadratic types of BBCs.

KEYWORDS

buck-boost converter (BBC), high gain buck-boost converter (HGBBC), small-signal analysis, Type III controller, voltage gain

1 | INTRODUCTION

As is well known, the buck-boost converter (BBC) is popular for step-down or step-up of the source voltage to a certain range and is utilized in various electrical/electronic systems.[1,2] BBC can be used for some important applications like switch mode power supplies, battery chargers, electric cars, traction systems, solar vehicles, fuel-cell systems, communication systems, defense equipment, radar power supply require the efficient, reliable, and compact DC–DC power

LIST OF SYMBOLS AND ABBREVIATIONS: C_1, C_2, capacitors; D_1, D_2, fast recovery power diodes; f_c, crossover frequency; f_s, switching frequency; i_{L1}, i_{L2}, inductors current; L_1, L_2, inductors; R, load resistor; r_{c1}, r_{c2}, equivalent series resistance of capacitors; r_{l1}, r_{l2}, equivalent series resistance of inductors; S_1, S_2, power switches (MOSFETs); T_s, total switching period; V_{C1}, V_{C2}, capacitors voltage; V_{con}, control voltage; V_{g1}, V_{g2}, gate pulses for power switches; V_{L1}, V_{L2}, inductors voltage; V_O, output (load) voltage; V_{ref}, reference input voltage; V_S, source voltage; V_{tri}, triangular waveform; δ, duty cycle ratio

converter.[3-5] BBC can also be applied in maximum power point tracking system for efficient power generation from solar Photovoltaic (PV) panel.[6] However, due to limited voltage gain (voltage conversion ratio), negative output voltage, and poor performance, its application is restricted when there is requirement of low or high voltage conversion of the converter.[7-11] On the other hand, isolated DC-DC power converters can produce high voltage gain, but due to the use of high-frequency transformers, the efficiency and power-handling capability will be reduced. The size and cost of the converter will also be increased. So, it is important to design a DC-DC converter which should have the features of high voltage gain with improved performance in terms of efficiency, dynamic response, and percentage ripple content for replacing the conventional BBC. To satisfy the aforesaid features of Switch Mode Power Converter (SMPC), the topologies of the converter attract a great deal of attention and many researchers have been proposed some modified topology of BBC. Tri-state buck-boost converter (TBBC) topology has been reported in Rana et al,[12] which improved the dynamic response of the converter by inserting a freewheeling circuit in the converter. The voltage gain of TBBC is higher than the voltage gain of conventional BBC. However, due to the use of freewheeling circuit, the efficiency of the converter is decreased and the complexity in the control circuit is increased. On the basis of Cuk converter topology, a single power switch-based BBC has been proposed in Ajami et al,[13] which has the advantages of lower ripple content in load voltage (output voltage) and minimum electromagnetic interference. But, the converter has limited voltage gain, complex structure due to its seventh-order circuit, and both source and load voltages are in opposite polarity. To enhance the voltage gain of conventional BBC, some modified converter topologies have been reported in previous studies.[14-16] Transformerless buck-boost converter (TLBBC) with positive output voltage and improved efficiency has been reported in Miao et al.[14] In TLBBC, an extra switching circuit is inserted into the conventional two switches-based BBC, and the voltage gain of this converter is the squared times the voltage gain of the conventional BBC. But, due to insertion of this extra switching circuit, the dynamic performance of TLBBC is reduced and ripple content in output voltage is also increased. Single-switch quadratic buck-boost converter (SSQBBC) with continuous input port current and continuous output port current has been proposed in Zhang et al.[15] The voltage gain of SSQBBC is also the squared times the voltage gain of the conventional BBC, and its source and load voltages are in the opposite polarity (negative load voltage). However, due to the use of more number of circuit elements, the order and complexity of the converter is increased as well as efficiency is decreased. Recently, a negative output buck-boost converter (NOBBC) with wide conversion ratio has been reported in Ding and Wang.[16] The voltage gain of NOBBC is improved but its source and load terminals are in the opposite polarity. The power efficiency of the converter is also poor.

To overcome such problems, a high-gain buck-boost converter (HGBBC) has been proposed and developed in this work. The power circuit of proposed HGBBC (shown in Figure 1) is developed by meaningful interchanging the position of the components of the existing converter (TLBBC[14]). In the proposed converter, the second inductor is connected in parallel with the load, which acts like a filter element in the output side of the converter and also minimizes the ripple content in the load voltage. But, in case of existing TLBBC, the second inductor is connected in series with the source, which draws excess current from the source and due to presence of parasitic element of the inductor, power loss is increased. The proposed converter having lesser number of circuit elements, and hence the complexity and order of the converter has been reduced. The efficiency, closed-loop dynamic response, and percentage ripple content in the load voltage of the proposed converter has also been improved. The ideal steady-state voltage gain of HGBBC has been derived and it appears that the obtained voltage gain is the squared times the voltage gain of the conventional BBC. The polarity of source voltage and load voltage are in same polarity (ie, noninverting polarity). The small-signal analysis of HGBBC has been established by using state-space averaging (SSA) technique[17-19] to find out the control-to-output transfer function of the proposed converter. It is found that right-half-plane (RHP) zero appeared in the obtained transfer function of HGBBC. To overcome the limited bandwidth due to RHP zero, an optimized Type III controller has been designed utilizing "*K-factor*" method[20-22] and particle swarm optimization (PSO) technique[23,24] for closed-loop control of HGBBC.

The performance comparisons between the proposed HGBBC and two other quadratic types of BBCs (TLBBC[14] and SSQBBC[15]) have been carried out in terms of efficiency and dynamic response. From the obtained results, it appears that

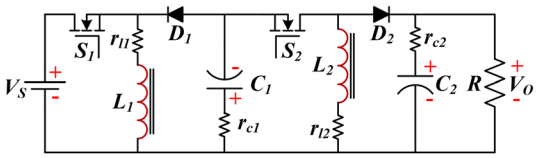

FIGURE 1 Power circuit of the proposed high-gain buck-boost converter (HGBBC)

HGBBC has achieved better performance than TLBBC and SSQBBC. The percentage ripple content in the load voltage of HGBBC and TLBBC has been investigated. It is found that the percentage ripple content in the load voltage of HGBBC is lesser than TLBBC.

The other part of the paper is organized as follows: The steady-state analysis of the proposed HGBBC is described in Section 2. The small-signal analysis of HGBBC is presented in Section 3. Optimized Type III controller design is described in Section 4. Simulated results are presented in Section 5. Hardware setup of closed-loop HGBBC and experimental results are given in Section 6. Comparative analyses of the proposed HGBBC and other two existing quadratic types of BBCs (TLBBC and SSQBBC) are given in Section 7. Finally, conclusion and some real-time applications of the proposed HGBBC are given in Section 8.

2 | STEADY-STATE ANALYSIS OF HGBBC

2.1 | Description of power circuit

The power circuit of the proposed HGBBC is shown in Figure 1,[1] where two power switches/Metal Oxide Semiconductor Field Effect Transistor (MOSFET) (S_1 and S_2) operate synchronously, ie, both switches will be turned on/off at the same time. The power circuit comprises of two power switches/MOSFETs (S_1 and S_2), two fast recovery power diodes (D_1 and D_2), two energy storage inductors (L_1 and L_2), two capacitors (C_1 and C_2), and a load resistor (R). V_S is the source voltage and V_O is the output voltage across the load (R) of the converter. r_{l1}, r_{l2}, r_{c1}, and r_{c2} are the equivalent series resistance (ESR) of inductors (L_1 and L_2) and capacitors (C_1 and C_2), respectively.

2.2 | Different modes of operation

The proposed HGBBC operates in two different states in continuous conduction mode (CCM) during steady state. In this subsection, the different operating modes are analyzed to realize how the proposed converter operates in that specific operating mode. The equivalent circuits of HGBBC corresponding to the two different operating modes are presented in Figure 2A and 2B, respectively. According to the operating modes of HGBBC, the theoretical time domain waveforms of two inductors current (i_{L1} and i_{L2}), two inductors voltage (V_{L1} and V_{L2}), and two gate pulses (V_{g1} and V_{g2}) are presented in Figure 3. Where, δ is the duty cycle ratio and T_s is the one complete switching cycle of the converter. The switching logic of HGBBC associated to the different operating modes is given in Table 1.

2.2.1 | Mode I operation

The equivalent circuit of HGBBC during Mode I operation is presented in Figure 2A. Here, both switches (S_1 and S_2) are turned on and both diodes (D_1 and D_2) are turned off simultaneously. Inductor L_1 is getting charged through source voltage V_S. Capacitor C_1 is discharged, and inductor L_2 is getting charged. Capacitor C_2 is discharging through load R and maintains the constant output voltage V_O. By applying Kirchhoff's voltage law (KVL) in the circuit given in

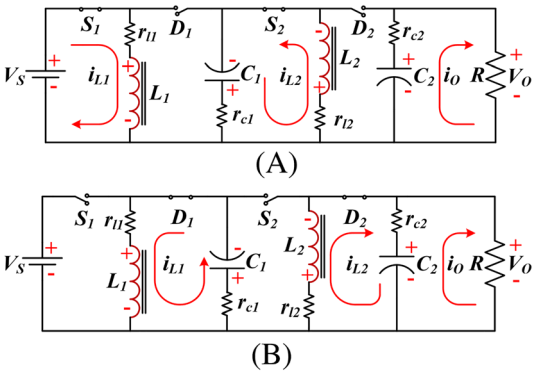

FIGURE 2 Equivalent circuit of high-gain buck-boost converter (HGBBC) during (A) Mode I and (B) Mode II operations

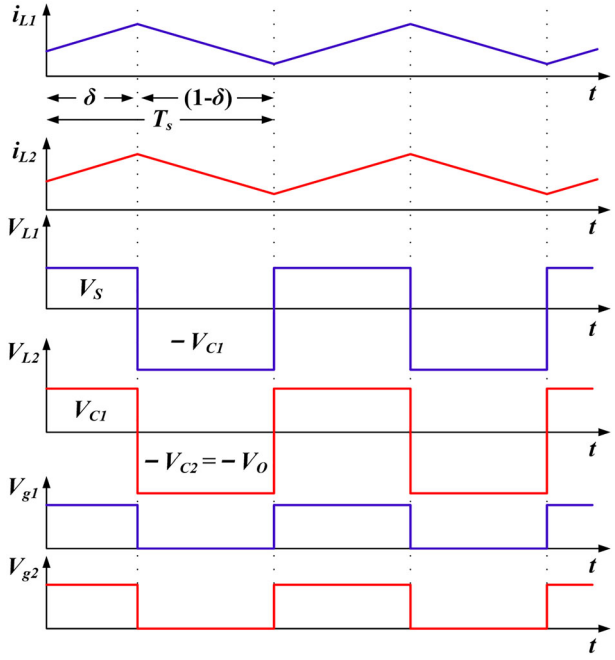

FIGURE 3 Theoretical time-domain waveforms of two inductors current (i_{L1} and i_{L2}), two inductors voltage (V_{L1} and V_{L2}) and two gate pulses (V_{g1} and V_{g2})

TABLE 1 Switching logic of HGBBC

Operating Mode	S_1	S_2	D_1	D_2
Mode I	ON	ON	OFF	OFF
Mode II	OFF	OFF	ON	ON

Abbreviation: HGBBC, high-gain buck-boost converter.

Figure 2A, the characteristics voltage equations of inductors and capacitors of the converter during Mode I operation (in ideal case) can be written as

$$V_{L1} = V_S, \tag{1}$$

$$V_{L2} = V_{C1}, \tag{2}$$

$$V_{C2} = V_O. \tag{3}$$

2.2.2 | Mode II operation

Mode II operation is just the complementary form of Mode I operation. Here, both switches (S_1 and S_2) are turned off and both diodes (D_1 and D_2) are turned on simultaneously. The equivalent circuit of HGBBC during Mode II operation is presented in Figure 2B. During this mode, the stored energy of inductor L_1 is dissipated across the capacitor C_1, and thus C_1 is getting charged. The stored energy of inductor L_2 is dissipated across capacitor C_2 and load R. Thus, C_2 is getting charged again and maintains the constant output voltage V_O. By applying KVL in the circuit presented in Figure 2B, the characteristics voltage equations of inductors and capacitors during Mode II operation (in ideal case) can be written as

$$V_{C1} = -V_{L1}, \tag{4}$$

$$V_{L2} = -V_{C2} = -V_O. \tag{5}$$

2.3 | Steady-state voltage gain

The steady-state voltage gain of HGBBC can be evaluated by using volt-second balance condition across each inductor voltages (V_{L1} and V_{L2}) over a period of time. During this derivation, the converter is considered as a lossless system and all the components of the converter are considered as ideal.

From the time-domain waveform of V_{L1} and applying volt-second balance condition across L_1, one can write (6).

$$V_S\delta T_s + (-V_{C1})(1-\delta)T_s = 0, \tag{6}$$

$$\Rightarrow V_{C1} = \{\delta/(1-\delta)\}V_S, \tag{7}$$

Similarly, from the time-domain waveform of V_{L2} and applying volt-second balance condition across L_2, (8) is derived.

$$V_{C1}\delta T_s + (-V_O)(1-\delta)T_s = 0, \tag{8}$$

$$\Rightarrow V_O = \{\delta/(1-\delta)\}V_{C1}. \tag{9}$$

Therefore, the final steady-state voltage gain of HGBBC can be obtained by putting (7) into (9) and given in (10).

$$V_O/V_S = \{\delta/(1-\delta)\}^2. \tag{10}$$

From (10), it is clear that the obtained voltage gain of the proposed HGBBC is the squared times the voltage gain of the conventional BBC. The source voltage of HGBBC will be step-down when δ 0.5 and step-up when δ 0.5.

2.4 | Selection of energy storage elements

2.4.1 | Selection of inductors (L_1 and L_2)

The expression for inductors (L_1 and L_2) current ripple Δi_{L1} and Δi_{L2} of HGBBC in ideal condition can be written as

$$\Delta i_{L1} = (V_S/L_1)\delta T_s = \left\{(1-\delta)^2 V_O T_s\right\}/\delta L_1, \tag{11}$$

$$\Delta i_{L2} = (V_{C1}/L_2)\delta T_s = \{(1-\delta)V_O T_s\}/L_2. \tag{12}$$

From (11) and (12), L_1 and L_2 value can be derived, which must satisfy the following criterion such that HGBBC may work in CCM. The expressions for L_1 and L_2 are presented in (13).

$$L_1 > RT_s(1-\delta)^3/2\delta;\ L_2 > RT_s(1-\delta)^2/2. \tag{13}$$

For discontinuous conduction mode (DCM) operation, the expressions for L_1 and L_2 can be written as follows:

$$L_1 < RT_s(1-\delta)^3/2\delta;\ L_2 < RT_s(1-\delta)^2/2. \tag{14}$$

2.4.2 | Selection of capacitors (C_1 and C_2)

The expression for capacitors (C_1 and C_2) of HGBBC in ideal condition can be established as

$$C_1 = \delta T_s V_O/\{R(1-\delta)\Delta V_{C1}\}, \tag{15}$$

$$C_2 = \delta T_s V_O/R\Delta V_{C2}. \tag{16}$$

If output voltage (V_O), duty cycle (δ), switching period (T_s), load (R), and capacitors voltage ripple (ΔV_{C1} and ΔV_{C2}) are known, then the values of C_1 and C_2 can be selected on the basis of (15) and (16).

3 | SMALL-SIGNAL ANALYSIS OF HGBBC

The small-signal analysis of HGBBC is described in this section. Here, the small-signal analysis has been established by using SSA technique to obtain the control-to-output (open-loop) transfer function of the converter. SSA is an approximation technique which converts nonliner time-varying converter model to an approximate liner converter model.[17-19] The state-space analysis of HGBBC is described below.

The proposed HGBBC operates in two modes during steady-state. Two inductors current (i_{L1} and i_{L2}) and two capacitors voltage (v_{C1} and v_{C2}) are defined as state variables. The different state equations of the converter according to the operating modes are presented in (17) and (18).

The state equations of HGBBC during Modes I and II operation can be obtained by using Kirchhoff's current law (KCL) and KVL of the circuits presented in Figure 2A and 2B, respectively.

Hence, the state equation corresponding to Mode I operation is presented in (17).

$$\begin{cases} \dfrac{di_{L1}}{dt} = -A_1 i_{L1} + A_2 V_S \\ \dfrac{di_{L2}}{dt} = -A_3 i_{L2} + A_4 v_{C1} \\ \dfrac{dv_{C1}}{dt} = -A_5 i_{L2} \\ \dfrac{dv_{C2}}{dt} = -A_6 v_{C2} \end{cases}. \tag{17}$$

And, the state equation corresponding to Mode II operation is presented in (18).

$$\begin{cases} \dfrac{di_{L1}}{dt} = -A_7 i_{L1} - A_2 v_{C1} \\ \dfrac{di_{L2}}{dt} = -A_8 i_{L2} - A_9 v_{C2} \\ \dfrac{dv_{C1}}{dt} = A_5 i_{L1} \\ \dfrac{dv_{C2}}{dt} = A_{10} i_{L2} - A_6 v_{C2} \end{cases}, \tag{18}$$

where $A_1 = r_{l1}/L_1$, $A_2 = 1/L_1$, $A_3 = (r_{l2}+r_{c1})/L_2$, $A_4 = 1/L_2$, $A_5 = 1/C_1$, $A_6 = 1/C_2(R+r_{c2})$, $A_7 = (r_{l1}+r_{c1})/L_1$, $A_8 = (r_{l2}R+r_{l2}r_{c2}+r_{c2}R)/L_2(R+r_{c2})$, $A_9 = R/L_2(R+r_{c2})$, and $A_{10} = R/C_2(R+r_{c2})$.

Now, SSA technique is introduced over one complete switching cycle of the converter. Thus, the average state equations of HGBBC can be written as

$$\frac{di_{L1}}{dt} = -A_1\delta i_{L1} + A_2\delta V_S - A_7(1-\delta)i_{L1} - A_2(1-\delta)v_{C1}, \tag{19}$$

$$\frac{di_{L2}}{dt} = -A_3\delta i_{L2} + A_4\delta v_{C1} - A_8(1-\delta)i_{L2} - A_9(1-\delta)v_{C2}, \tag{20}$$

$$\frac{dv_{C1}}{dt} = -A_5\delta i_{L2} + A_5(1-\delta)i_{L1}, \tag{21}$$

$$\frac{dv_{C2}}{dt} = -A_6\delta v_{C2} + A_{10}(1-\delta)i_{L2} - A_6(1-\delta)v_{C2}. \tag{22}$$

The small ac perturbations are applied into (19) to (22). The perturbed variables are defined as $i_{L1} = I_{L1} + \widetilde{i}_{L1}$, $i_{L2} = I_{L2} + \widetilde{i}_{L2}$, $v_{C1} = V_{C1} + \widetilde{v}_{C1}$, $v_{C2} = V_{C2} + \widetilde{v}_{C2}$, $v_O = V_O + \widetilde{v}_O$, and $\delta = \Delta + \widetilde{\delta}$. Here, the uppercase letters are indicated the steady-state DC quantities and small ac perturbed quantities are denoted by "~." Then, separating the DC and variable ac terms and ignoring the small-signal higher order expressions. Finally, by using Laplace transformation, the

control-to-output transfer function is derived. Thus, the obtained control-to-output ($V_O(s)/(s)$) transfer function of HGBBC is presented in (23).

$$T_{HGBBC}(s) = \frac{V_O(s)}{\Delta(s)} = \frac{(-X_1 s^3 + X_2 s^2 + X_3 s + X_4)(1 + r_{c2} C_2 s)}{s^4 + Y_1 s^3 + Y_2 s^2 + Y_3 s + Y_4}, \tag{23}$$

where $X_1 = B_{12}$, $X_2 = B_5 B_{11} - B_1 B_{12} - B_4 B_{12}$,

$X_3 = B_1 B_5 B_{11} - B_6 B_9 B_{11} - B_3 B_8 B_{12} - B_1 B_4 B_{12} - B_6 B_{10} B_{12}$,

$X_4 = B_3 B_5 B_8 B_{11} + B_2 B_6 B_8 B_{11} - B_1 B_6 B_9 B_{11} - B_3 B_4 B_8 B_{12} - B_1 B_6 B_{10} B_{12}$,

$Y_1 = A_6 + B_1 + B_4$, $Y_2 = B_1 B_4 + B_3 B_8 + B_6 B_{10} + A_6 B_1 + A_6 B_4 + B_7 B_{11}$,

$Y_3 = B_3 B_4 B_8 + B_1 B_6 B_{10} + A_6 B_3 B_8 + A_6 B_1 B_4 + A_6 B_6 B_{10} + B_1 B_7 B_{11}$, and

$Y_4 = A_6 B_1 B_6 B_{10} + A_6 B_3 B_4 B_8 + B_3 B_7 B_8 B_{11}$.

And, $B_1 = A_1\delta + A_7(1-\delta)$, $B_2 = I_{L1}(A_7 - A_1) + A_2(V_S + V_{C1})$, $B_3 = A_2(1-\delta)$,

$B_4 = A_3\delta + A_8(1-\delta)$, $B_5 = I_{L2}(A_8 - A_3) + A_4 V_{C1} + A_9 V_{C2}$, $B_6 = A_4\delta$, $B_7 = A_9(1-\delta)$,

$B_8 = A_5(1-\delta)$, $B_9 = A_5(I_{L1} + I_{L2})$, $B_{10} = A_5\delta$, $B_{11} = A_{10}(1-\delta)$, and $B_{12} = A_{10} I_{L2}$.

The steady-state value of capacitors voltage (V_{C1} and V_{C2}) and inductors current (I_{L1} and I_{L2}) can be calculated by solving (24) to (27).

$$V_{C1} = [-A_1\delta/\{A_2(1-\delta)\} - A_7/A_2] I_{L1} + \delta V_S/(1-\delta), \tag{24}$$

$$V_{C2} = A_{10}(1-\delta) I_{L2}/A_6, \tag{25}$$

$$I_{L1} = \delta I_{L2}/(1-\delta), \tag{26}$$

$$I_{L2} = \frac{A_2 \delta V_S}{\frac{A_1\delta^2}{(1-\delta)} + A_7\delta + \frac{A_2 A_3(1-\delta)}{A_4} + \frac{A_2 A_8 (1-\delta)^2}{A_4\delta} + \frac{A_2 A_9 A_{10}(1-\delta)^3}{A_4 A_6 \delta}}. \tag{27}$$

The converter parameters values are taken as $V_S = 10$ to 25 V, $V_O = 10$ to 25 V, $L_1 = L_2 = 250$ μH, $C_1 = C_2 = 470$ μF, $r_{l1} = r_{l2} = 0.2$ Ω, $r_{c1} = r_{c2} = 0.095$ Ω, $R = 50$ Ω, and switching frequency $f_s = 20$ kHz. For a particular operating point ($V_S = 10$ V, $V_O = 25$ V), the control-to-output transfer function of HGBBC can be derived from (23), and it is given in (28).

$$T_{HGBBC}(s) = \frac{V_O(s)}{\Delta(s)} = \frac{-0.10962(s - 48330)(s + 22400)(s^2 + 801.6s + 2.509 \times 10^6)}{s^4 + 2169s^3 + 6.951 \times 10^6 s^2 + 5.975 \times 10^9 s + 1.818 \times 10^{12}}. \tag{28}$$

From (28), it is clear that RHP zero appeared in the obtained transfer function of HGBBC. Therefore, to improve the overall performances of the converter, a generalized optimized Type III controller has been utilized.

4 | OPTIMIZED TYPE III CONTROLLER DESIGN

To study the closed-loop converter's dynamic performances, a generalized optimized Type III controller is implemented on the basis of conventional "*K-factor*" method[20-22] and PSO technique.[23,24] Similar specifications are considered in controller design procedure for three converters (ie, HGBBC, TLBBC, and SSQBBC) to achieve the comparable performances. The complete design procedure of the proposed Type III controller is described below.

The generalized transfer function of Type III controller is given as follows:

$$T_C(s) = \left\{ \left(1 + s/\omega_{c-z1,2}\right)^2 \right\} / \left\{ \left(s/\omega_{c-p0}\right)\left(1 + s/\omega_{c-p1,2}\right)^2 \right\} \tag{29}$$

Here, $\omega_{c\ -\ z1,2}$ and $\omega_{c\ -\ p1,2}$ are the frequencies of the double zero and double pole, respectively, of the proposed Type III controller, while $\omega_{c\ -\ p0}$ is the frequency of the single pole located at zero position.

In Type III controller, the pole at the origin provides a very high gain at low frequencies, and the pole-zero pairs reduce the phase shift between the frequency of the two zeros and the frequency of two poles as lead controller. So this controller may provide 0° to 180° "phase_boost" with zero steady-state error. The Type III controller is intended for switching converters that exhibit a –40-dB/decade roll-off above the poles of the output filter and a –180° phase lag. This extends the loop bandwidth. Type III controller network can achieve a very fast dynamic response, and they are commonly used for systems requiring very fast transient response.

The magnitude of the controller can be written as

$$|T_C(j\omega)| = \frac{\left|1 + j\frac{\omega}{\omega_{c-z1,2}}\right|\left|1 + j\frac{\omega}{\omega_{c-z1,2}}\right|}{\left|j\frac{\omega}{\omega_{c-p0}}\right|\left|1 + j\frac{\omega}{\omega_{c-p1,2}}\right|\left|1 + j\frac{\omega}{\omega_{c-p1,2}}\right|}. \tag{30}$$

The argument of the controller can be written as

$$\phi(T_C(j\omega)) = 2\tan^{-1}\left(\frac{\omega}{\omega_{c-z1,2}}\right) - 2\tan^{-1}\left(\frac{\omega}{\omega_{c-p1,2}}\right) - \frac{\pi}{2}. \tag{31}$$

Type III controller can provide maximum 180° phase_boost by varying the location of pole and zero. The frequency where maximum phase_boost can be obtained by taking the derivate of (31) with respect to frequency f.

$$\frac{d}{df}\phi(T_C(j\omega)) = \frac{d}{df}\left(2\tan^{-1}\left(\frac{f}{f_{c-z1,2}}\right) - 2\tan^{-1}\left(\frac{f}{f_{c-p1,2}}\right)\right). \tag{32}$$

$$or,\ \frac{2}{f_{c-z1,2}\left(\frac{f^2}{f_{c-z1,2}^2} + 1\right)} - \frac{2}{f_{c-p1,2}\left(\frac{f^2}{f_{c-p1,2}^2} + 1\right)} = 0. \tag{33}$$

By solving f from (33), the maximum phase_boost can be obtained at the "geometric mean of the double zero-double pole" frequencies in the controller and can be written in (34) as follows:

$$f_{c-\max} = \sqrt{f_{c-z1,2} \times f_{c-p1,2}}. \tag{34}$$

Therefore, $f_{c\text{-}max}$ is considered as crossover frequency (f_c) of Type III controller.

Now, introducing *K-factor* of Type III controller, which is the ratio between frequencies of double pole to double zero. The relationship between phase_boost and "*K*" can be established as follows:

$$phase\_boost = 2\left(\tan^{-1}\sqrt{K} - \tan^{-1}\frac{1}{\sqrt{K}}\right). \tag{35}$$

The expression of K can be deduced from (35) and it is given in (36).

$$K = \left\{\tan\left(\frac{phase\_boost}{4} + \frac{\pi}{4}\right)\right\}^2. \tag{36}$$

Equation (36) is known as *K-factor* of Type III controller.

Therefore, the double zero and double pole position can be deduced from (37) and (38) for a particular crossover-frequency (f_c) and necessary phase_boost.

$$f_{c-z1,2} = f_c/\sqrt{K} = f_c/\tan\{(phase\_boost + \pi)/4\}. \tag{37}$$

$$\text{And, } f_{c-p1,2} = f_c \times \sqrt{K} = f_c \times \tan\{(phaseboost + \pi)/4\}. \tag{38}$$

Midband gain of the controller can be derived as follows.

The controller transfer function (29) can be written as

$$T_C(s) = \frac{s}{\omega_{c-z1}} \times \frac{(1+\omega_{c-z1}/s)(1+s/\omega_{c-z2})}{(s/\omega_{c-p0})(1+s/\omega_{c-p1})(1+s/\omega_{c-p2})},$$

$$T_C(s) = G_{c-O} \times \frac{(1+\omega_{c-z1}/s)(1+s/\omega_{c-z2})}{(1+s/\omega_{c-p1})(1+s/\omega_{c-p2})}, \tag{39}$$

where $G_{c\text{-}O}$ is the midband gain of the controller and $G_{c\_O} = \omega_{c\_p0}/\omega_{c\_z1}$. The value of ω_{c_p0} depends on the required gain at crossover frequency. $G_{c\text{-}O}$ can be written as

$$G_{c-O} = G_c \times \frac{\sqrt{1+\left(\frac{\omega_c}{\omega_{c-p1}}\right)^2}\sqrt{1+\left(\frac{\omega_c}{\omega_{c-p2}}\right)^2}}{\sqrt{1+\left(\frac{\omega_{c-z1}}{\omega_c}\right)^2}\sqrt{1+\left(\frac{\omega_c}{\omega_{c-z2}}\right)^2}}, \tag{40}$$

where G_c is the gain of the selected crossover frequency f_c.

$$\omega_{c-p0} = G_c \times \frac{\omega_{c-z1}\sqrt{1+\left(\frac{\omega_c}{\omega_{c-p1}}\right)^2}\sqrt{1+\left(\frac{\omega_c}{\omega_{c-p2}}\right)^2}}{\sqrt{1+\left(\frac{\omega_{c-z1}}{\omega_c}\right)^2}\sqrt{1+\left(\frac{\omega_c}{\omega_{c-z2}}\right)^2}}. \tag{41}$$

If double poles and zeros are considered at the same point, the formula becomes

$$\omega_{c-p0} = G_c \times \frac{\omega_{c-z1,2}\left(\omega_{c-p1,2}^2 + \omega_c^2\right)}{\omega_{c-p1,2}^2\sqrt{1+\left(\frac{\omega_{c-z1,2}}{\omega_c}\right)^2}\sqrt{1+\left(\frac{\omega_c}{\omega_{c-z1,2}}\right)^2}}. \tag{42}$$

Now, it is assumed that the converter has −10 dB gain deficit at $f_c = 1$ kHz (which is much less than the switching frequency 20 kHz of the converter) and necessary phase_boost is 150°. From (37) and (38), the position of double zero and double pole are derived and given in (43) and (44).

$$f_{c-z1,2} = 1000/\tan\{(150^o + 180^o)/4\} = 131.65\ \ Hz, \tag{43}$$

$$f_{c-p1,2} = 1000 \times \tan\{(150^o + 180^o)/4\} = 7.596\ \ kHz. \tag{44}$$

At 1 kHz selected "f_c," gain (G_c) must be −10 dB. Hence, 0-dB crossover pole location is derived as follows:

$$f_{c-p0} = \frac{G_c \times f_{c-z1,2} \times \left(f_{c-p1,2}^2 + f_c^2\right)}{f_{c-p1,2}^2 \times \left(\sqrt{\left(f_{c-z1,2}/f_c\right)^2 + 1}\right) \times \left(\sqrt{\left(f_c/f_{c-z1,2}\right)^2 + 1}\right)} = 54.81\ \ Hz. \tag{45}$$

After optimizing of the controller parameters by using of PSO technique, the final transfer function of designed Type III controller is given in (46).

$$T_C(s) = \frac{174.19(s+720)^2}{s(s+6010)^2}. \tag{46}$$

The description of PSO technique is given in the following flowchart (shown in Figure 4).

The fitness function for PSO can be written as

$$fit(t) = \int_0^\tau t|e(t)|dt, \tag{47}$$

where τ is the steady-state value.

The position of the qth agent among n_p total number of population is defined as

$$Y_q = \left(Y_q^1, Y_q^2, Y_q^3, ...Y_q^d, ...Y_q^n\right) \quad \text{for } q\ 1,\ 2,\ 3,\ ....., np\,, \tag{48}$$

where Y_q^d is the position of qth particle vector in the dth dimension and n is the total number of dimensions.

Each particle vector of population n_p represents five parameters of Type III controller (Y_q^1 = controller gain, Y_q^2 = first zero position, Y_q^3 = second zero position, Y_q^4 = first pole position, and Y_q^5 = second pole position).

The velocity vector for each dimension of the particle vector can be written as

$$v_q = \left(v_q^1, v_q^2, v_q^3, ...v_q^d, ...v_q^n\right). \tag{49}$$

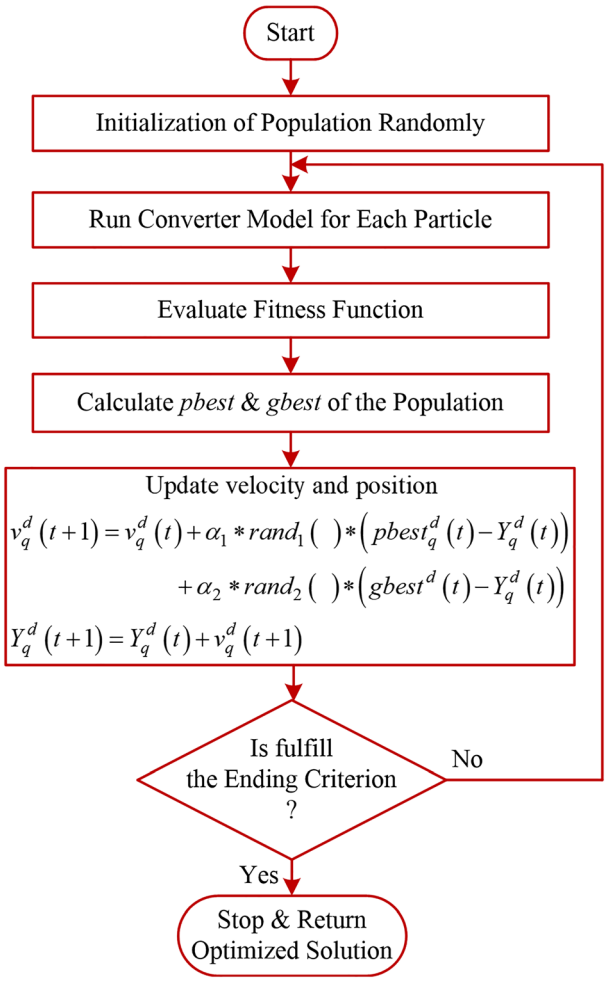

FIGURE 4 Flowchart for Particle Swarm Optimization (PSO) algorithm

The *pbest* and *gbest* position for each particle can be written as

$$pbest_q = \left(pbest_q^1, pbest_q^2, pbest_q^3, ...pbest_q^d, ...pbest_q^n\right), \tag{50}$$

$$gbest_q = \left(gbest^1, gbest^2, gbest^3, ...gbest^d, ...gbest^n\right). \tag{51}$$

The expression for the velocity and position vector of PSO can be written as follows:

$$v_q^d(t+1) = v_q^d(t) + \alpha_1 * \text{rand}_1() * \left(pbest_q^d(t) - Y_q^d(t)\right) + \alpha_2 * \text{rand}_2() * \left(gbest^d(t) - Y_q^d(t)\right), \tag{52}$$

$$Y_q^d(t+1) = Y_q^d(t) + v_q^d(t+1), \tag{53}$$

where α_1 and α_2 are known as the learning rate constant. t is the number of current iteration and $rand_1()$ and $rand_2()$ are uniformly distributed random numbers in the range [0, 1]. The flowchart of the PSO algorithm is presented in Figure 4.

The bode diagram of HGBBC with and without developed Type III controller is shown in Figure 5. The performance specifications of HGBBC are summarized in Table 2. It is clear that the proposed HGBBC with developed controller exhibits superior stability characteristics in closed-loop with improved gain margin (GM) and phase margin (PM).

5 | SIMULATION RESULTS AND DISCUSSIONS

Extensive simulations have been carried out through MATLAB simulation to validate the advantages of the proposed HGBBC over other two existing quadratic types of BBCs (TLBBC[14] and SSQBBC[15]). The load regulation and reference input voltage tracking performance have been tested and compared with TLBBC and SSQBBC.

The comparative load regulation performance test of HGBBC, TLBBC, and SSQBBC has been conducted and is presented in Figure 6A and 6B. During this test ±50% step disturbance is applied in the load (R) and captured

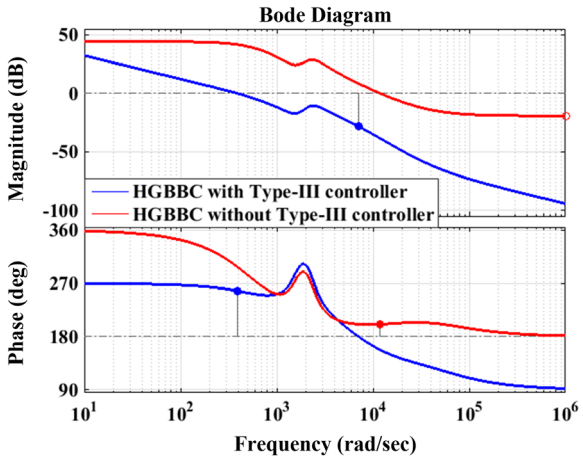

FIGURE 5 Bode diagram of high-gain buck-boost converter (HGBBC) with and without Type III controller

TABLE 2 Performance specifications of HGBBC

Specifications	HGBBC Without Type III Controller	HGBBC With Type III Controller
GM	19.2 dB	28.4 dB
PM	20.9°	77.2°
GCF	11 900 rad/s	389 rad/s
PCF	Infinity	7080 rad/s

Abbreviations: GCF, gain crossover frequency; GM, gain margin; HGBBC, high-gain buck-boost converter; PCF, phase crossover frequency; PM, phase margin.

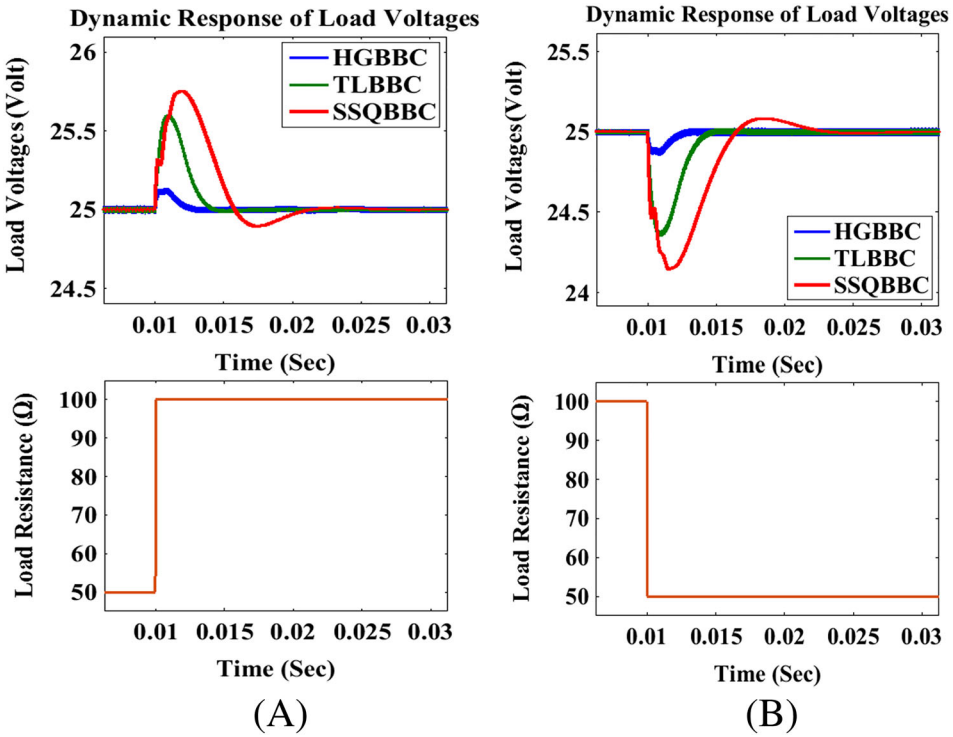

FIGURE 6 Dynamic response of load voltages when (A) +50% and (B) −50% step disturbance is applied in the load resistance (R)

the load voltages dynamic response. By inspection, one can say the proposed HGBBC has achieved better load regulation performance than TLBBC and SSQBBC. The reference input voltage tracking performance test of load voltages of the proposed HGBBC, TLBBC, and SSQBBC has been carried out by changing ±20% of reference input voltage and is presented in Figure 7A and 7B. It is observed that the tracking performance of load voltage of HGBBC is showing better than TLBBC and SSQBBC. In both cases, the load voltage dynamic response of HGBBC is showing the minimum overshoot, faster rise time, lesser setting time, and zero steady-state error. Simulated time-domain waveforms of inductors current and inductors voltage (i_{L1}, i_{L2}, V_{L1}, and V_{L2}) along with two gate pulses for power switches S_1 and S_2 (V_{g1} and V_{g2}) of HGBBC during boost mode and buck mode are presented in Figure 8A and 8B. The steady-state waveforms of load voltage (V_O), capacitor voltage (V_{C1}), and source voltage (V_S) of the proposed HGBBC for a particular operating point during boost mode as well as buck mode have been observed and are presented in Figure 9A and 9B, respectively.

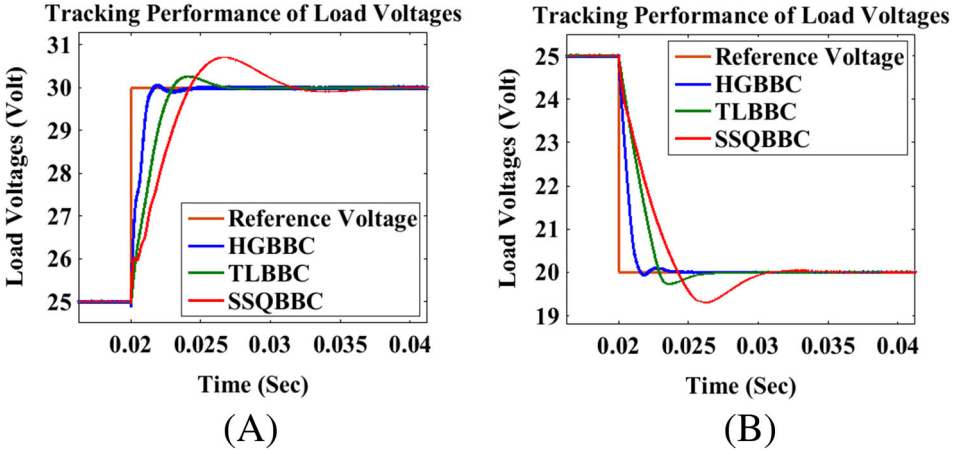

FIGURE 7 Tracking performance of load voltages when (A) +20% and (B) −20% step disturbance is applied in the reference input voltage

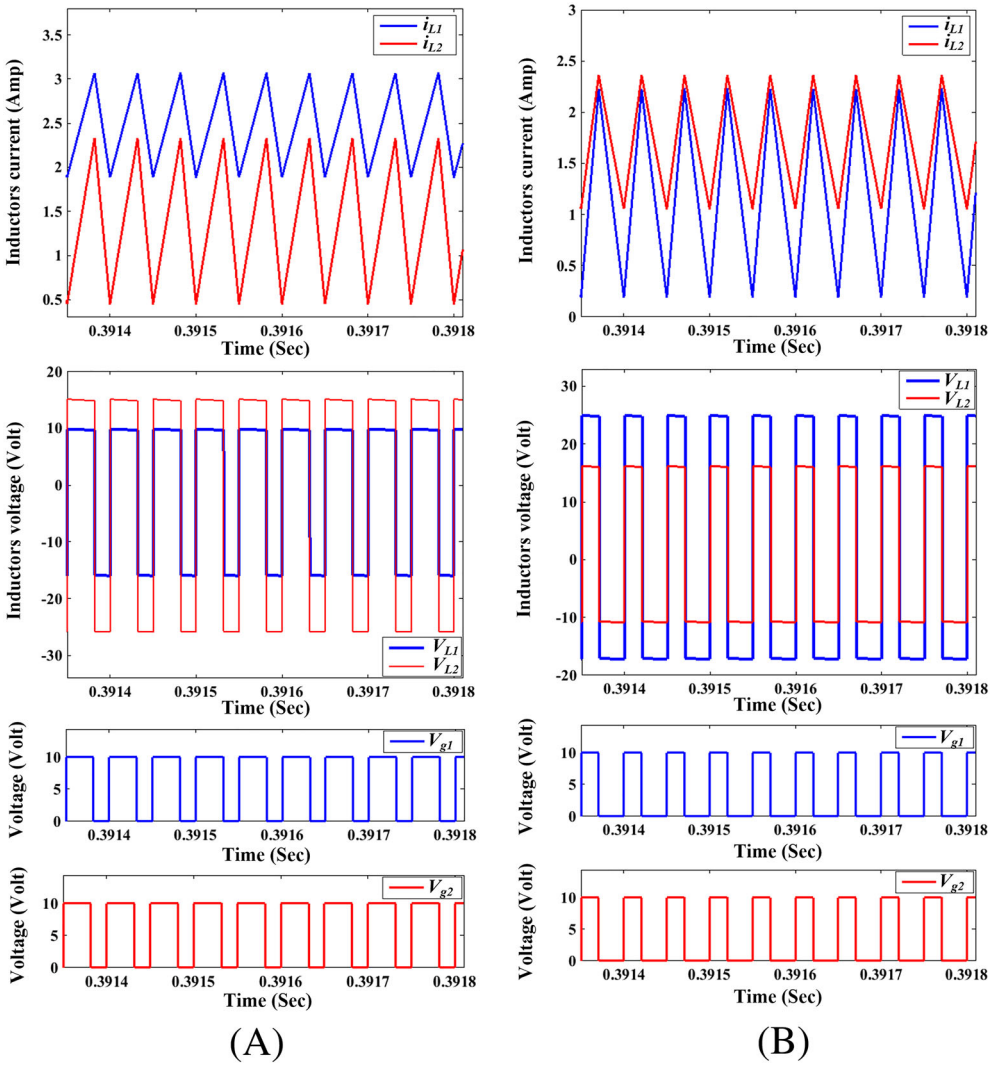

FIGURE 8 Simulated time-domain waveforms of inductors current (i_{L1} and i_{L2}) and inductors voltage (V_{L1} and V_{L2}) along with two gate pulses (V_{g1} and V_{g2}) of high-gain buck-boost converter (HGBBC) during (A) boost mode and (B) buck mode

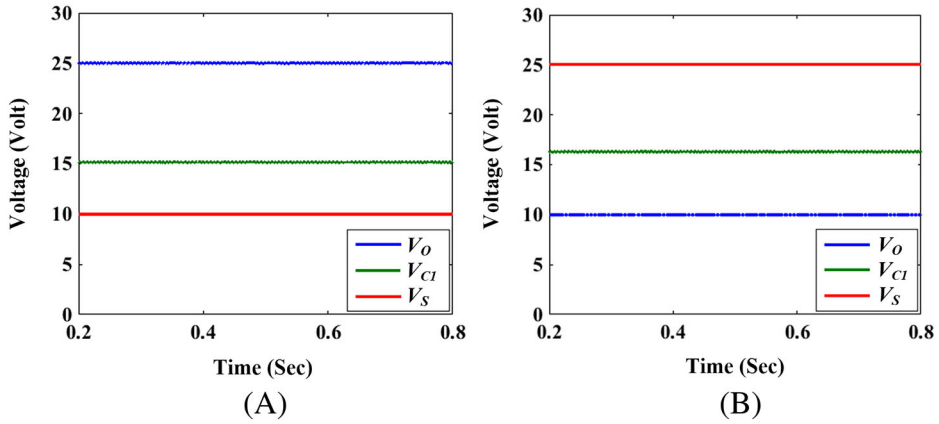

FIGURE 9 Steady-state waveforms of load voltage (V_O), capacitor voltage (V_{C1}), and source voltage (V_S) of high-gain buck-boost converter (HGBBC) during (A) boost mode and (B) buck mode

6 | EXPERIMENTAL RESULTS AND DISCUSSIONS

6.1 | Circuit diagram and hardware setup

An experimental setup of 50 W maximum power rating has been fabricated in the laboratory to validate the simulation results of the proposed HGBBC. The complete closed-loop converter's circuit diagram is presented in Figure 10A. The

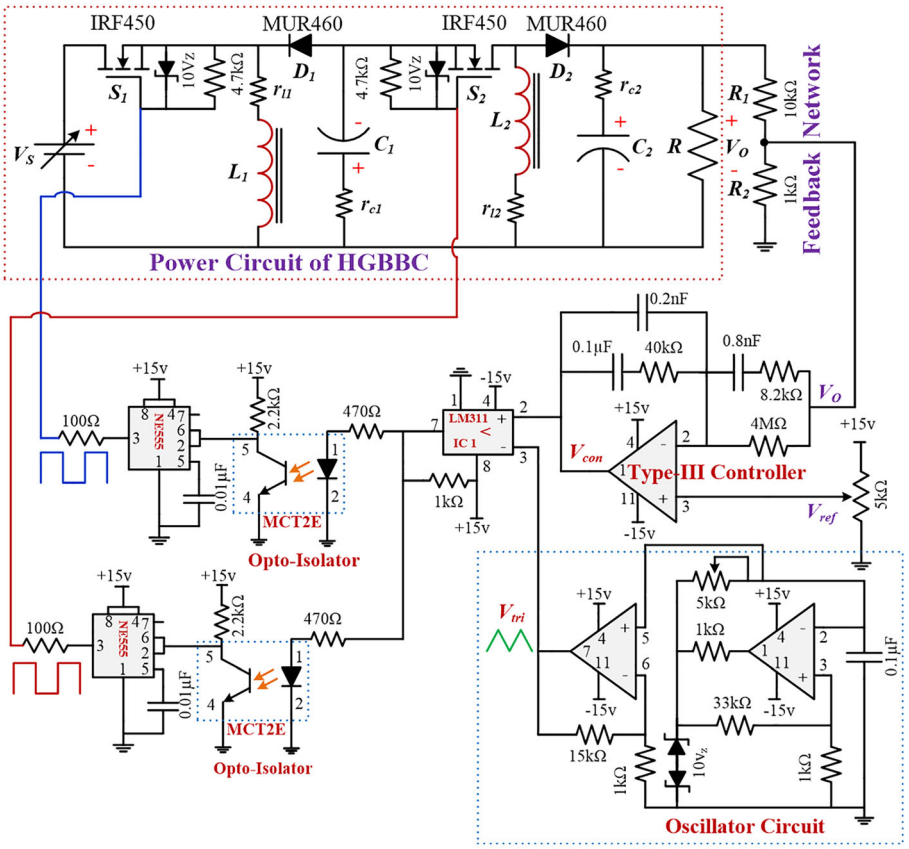

(A)

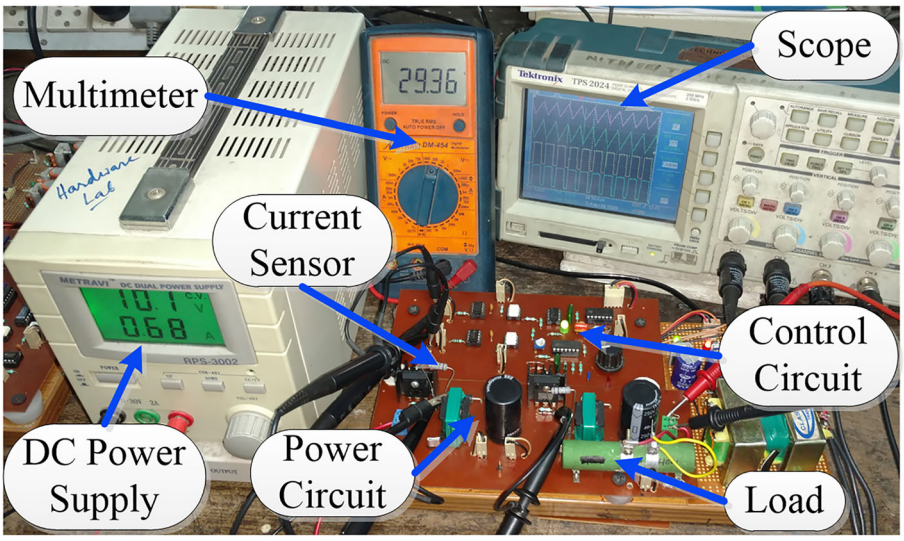

(B)

FIGURE 10 (A) Circuit diagram of closed-loop high-gain buck-boost converter (HGBBC) and (B) Hardware setup of HGBBC

whole circuitry has been assembled in a single printed circuit board (PCB) and the overall hardware setup is shown in Figure 10B.

The power circuit of HGBBC consists of a variable DC power supply (V_S = 0-30 V), two inductors (250 μH), two capacitors (470 μF/250 V), two power MOSFETs (IRF450), two fast recovery power diodes (MUR460), and a load (rheostat) of 220 Ω/100 W.

An op-amp-based oscillator circuit is used to generate the triangular waveform (V_{tri}) in the control circuit. The frequency of the generated triangular waveform is fixed at 20 kHz. The actual load voltage (V_O) of the converter is scaled down by using a voltage divider circuit (R_1 and R_2) then sensed for comparing with reference input voltage (V_{ref}) to produce the error signal. The generated error signal is passed through the Type III controller which produces control voltage (V_{con}). A comparator (LM311) is used to compare the triangular waveform (V_{tri}) with control voltage (V_{con}) and generates the PWM signal. The generated PWM signal is applied to drive the gates of two power MOSFETs (S_1 and S_2) after passing through the respective opto-isolators (MCT2E) and gate drivers (NE555).

6.2 | Experimental results

It has been observed from the simulation results (Figures 6 and 7) that the proposed HGBBC is performed better as compared with TLBBC and SSQBBC. In order to validate the simulation results, experimental performance test of HGBBC has been carried out in laboratory under various cases, ie, change in load (R), change in source voltage (V_S), and change in reference voltage. The load voltage (V_O) dynamic responses of HGBBC have been captured in all cases and are presented in Figures 11, 12, and 13. It appears from the obtained experimental results (Figures 11, 12, and 13) that the proposed HGBBC

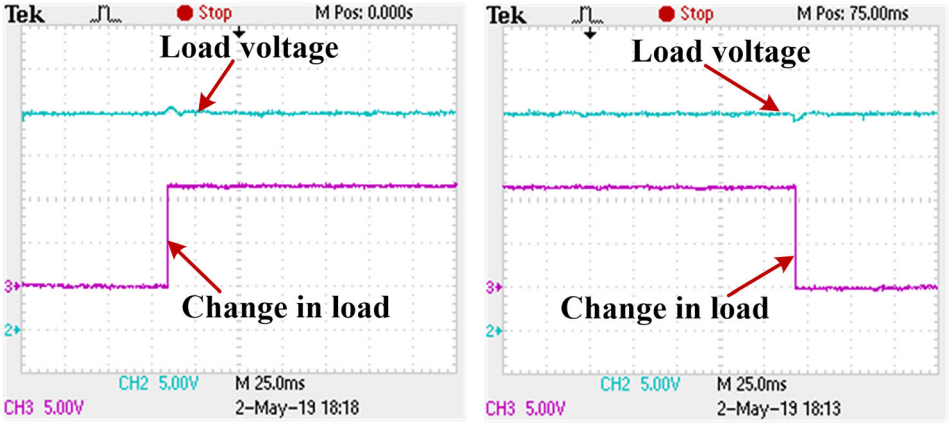

FIGURE 11 Dynamic response of load voltage (V_O) of high-gain buck-boost converter (HGBBC) when (A) +50% and (B) −50% step change is applied in load (R) [CH2: V_O, CH3: voltage drop across shorted load resistance (R)]

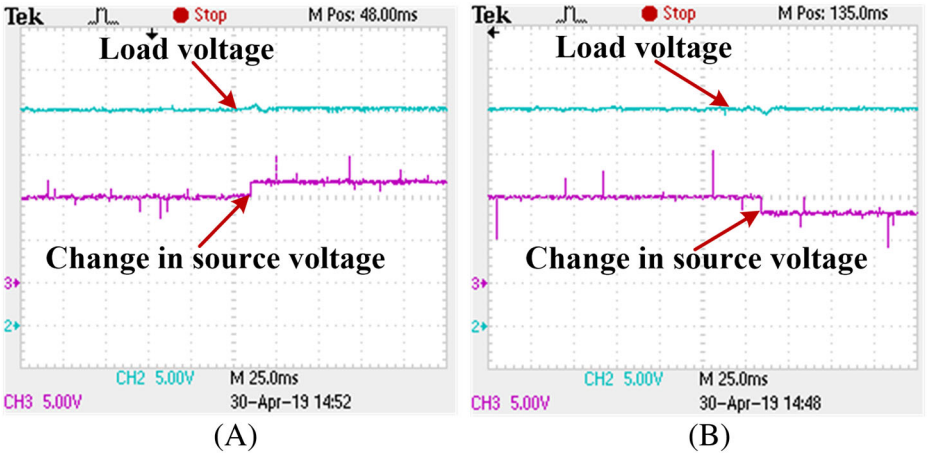

FIGURE 12 Dynamic response of load voltage (V_O) of high-gain buck-boost converter (HGBBC) when (A) +20% and (B) −20% step change is applied in source voltage (V_S) [CH2: V_O, CH3: V_S]

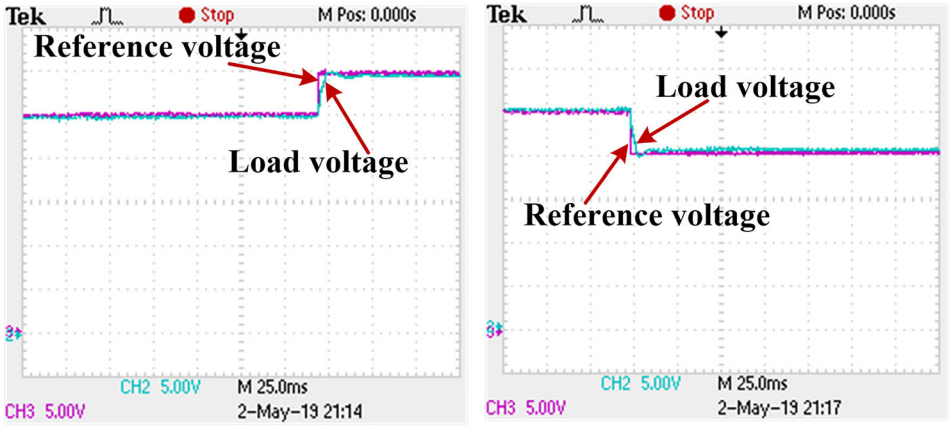

FIGURE 13 Dynamic response of load voltage (V_O) of high-gain buck-boost converter (HGBBC) when (A) +20% and (B) −20% step change is applied in reference voltage [CH2: V_O, CH3: Reference voltage]

exhibits superior and robust performance under all operating conditions with minimum overshoot, faster rise time, lesser setting time, and zero steady-state error. The steady-state time-domain waveforms of inductors current and inductors voltage (i_{L1}, i_{L2}, V_{L1}, and V_{L2}) along with two gate pulses for the power MOSFETs (V_{g1} and V_{g2}) of HGBBC during boost mode and buck mode are presented in Figures 14 and 15, respectively. Two current probes (Tektronix A622) are used to measure the two inductors current (i_{L1} and i_{L2}) patterns. From Figures 8, 14, and 15, it appears that the simulation and experimental time-domain waveforms of the proposed HGBBC are similar. The experimental steady-state waveforms of load voltage (V_O), source voltage (V_S), capacitor voltage (V_{C1}), and gate pulse for switch S_1 (V_{g1}) of the proposed converter for a particular operating point during boost mode as well as buck mode have been observed and are illustrated in Figure 16A and 16B, respectively.

7 | COMPARISON BETWEEN THE PROPOSED HGBBC AND OTHER EXISTING CONVERTERS

This section describes the comparison between the proposed HGBBC and two other existing quadratic types of BBCs (TLBBC and SSQBBC) based on the percentage efficiency, ripple content in the load voltage, and number of components that are used in the power circuits of the converters.

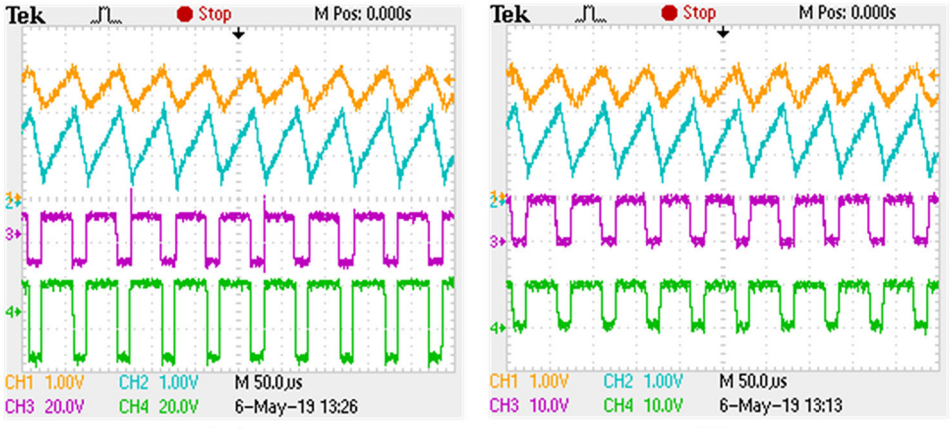

FIGURE 14 Experimental time-domain waveforms of high-gain buck-boost converter (HGBBC) during boost mode (A) CH1: inductor current (i_{L1}), CH2: inductor current (i_{L2}), CH3: inductor voltage (V_{L1}), CH4: inductor voltage (V_{L2}) and (B) CH1: inductor current (i_{L1}), CH2: inductor current (i_{L2}), CH3: gate pulse for S_1 (V_{g1}), CH4: gate pulse for S_2 (V_{g2})

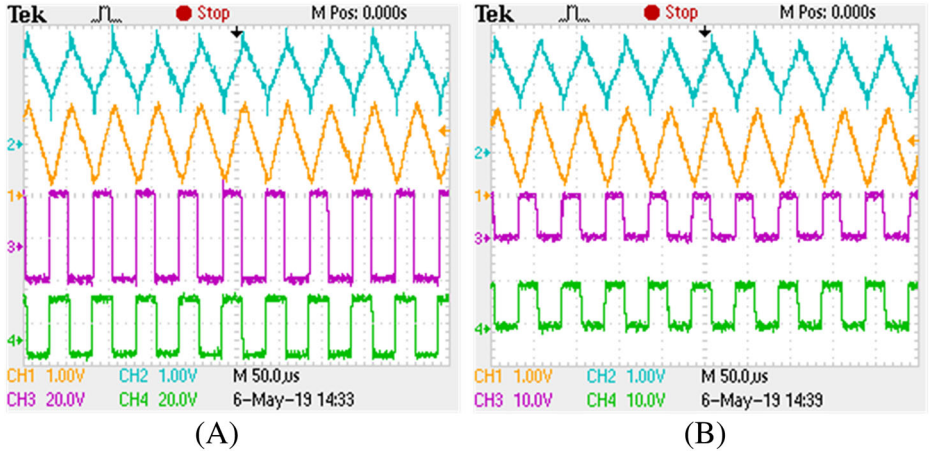

FIGURE 15 Experimental time-domain waveforms of high-gain buck-boost converter (HGBBC) during buck mode (A) CH1: inductor current (i_{L1}), CH2: inductor current (i_{L2}), CH3: inductor voltage (V_{L1}), CH4: inductor voltage (V_{L2}) and (B) CH1: inductor current (i_{L1}), CH2: inductor current (i_{L2}), CH3: gate pulse for S_1 (V_{g1}), CH4: gate pulse for S_2 (V_{g2})

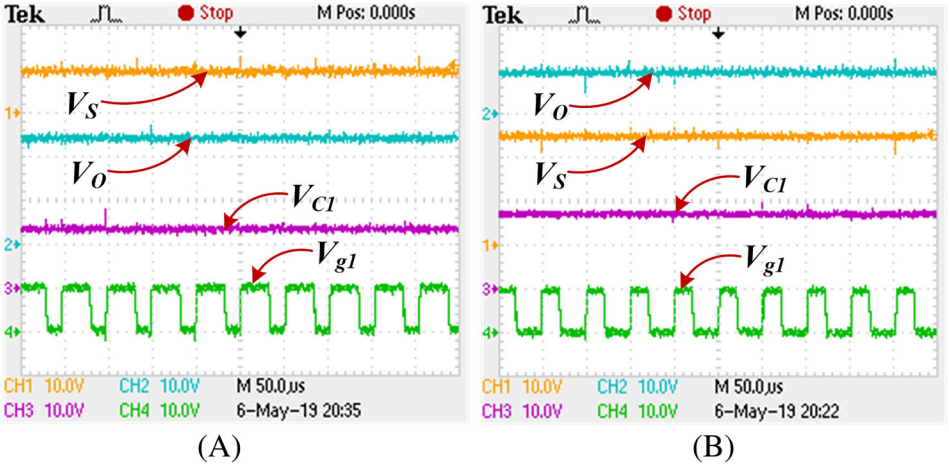

FIGURE 16 Experimental steady-state waveforms of source voltage (V_S), load voltage (V_O), capacitor voltage (V_{C1}) and gate pulse for S_1 (V_{g1}) of high-gain buck-boost converter (HGBBC) during (A) boost mode and (B) buck mode [CH1: V_S, CH2: V_O, CH3: V_{C1} and CH4: V_{g1}]

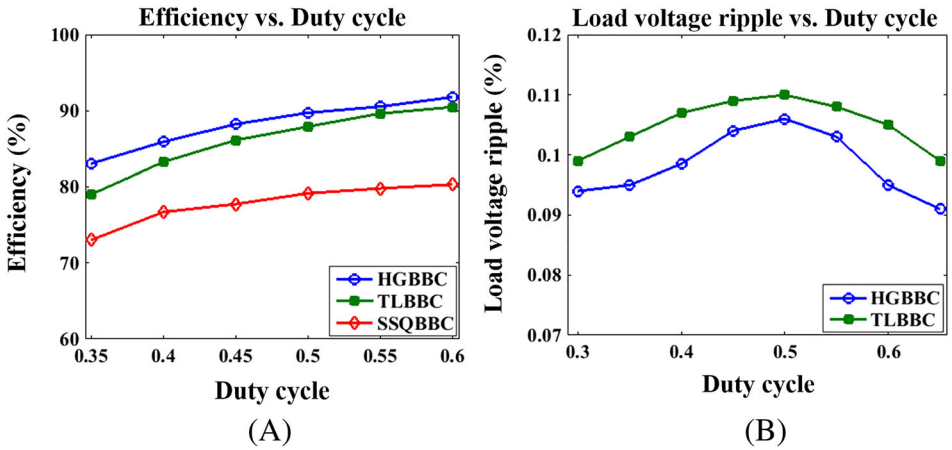

FIGURE 17 (A) Percentage efficiency comparison between high-gain buck-boost converter (HGBBC), transformerless buck-boost converter (TLBBC), and single-switch quadratic buck-boost converter (SSQBBC) and (B) load voltage (V_O) ripple comparison between HGBBC and TLBBC

TABLE 3 Overall comparison between the proposed HGBBC and other existing converters

Topology	TLBBC	SSQBBC	HGBBC
Power switches	2	1	2
Power diodes	2	5	2
Inductors	2	3	2
Capacitors	2	3	2
Voltage gain	$\left(\frac{\delta}{1-\delta}\right)^2$	$\left(\frac{\delta}{1-\delta}\right)^2$	$\left(\frac{\delta}{1-\delta}\right)^2$
Order of the converters	Fourth order (four energy storage elements)	Sixth order (six energy storage elements)	Fourth order (four energy storage elements)

Abbreviations: HGBBC, high-gain buck-boost converter; TLBBC, transformerless buck-boost converter; SSQBBC, single-switch quadratic buck-boost converter.

The percentage efficiency of three converters (HGBBC, TLBBC, and SSQBBC) has been measured by varying the duty cycle and prepared a graph between percentage efficiency vs duty cycle which is illustrated in Figure 17A. It appears that HGBBC is more energy efficient as compared with TLBBC and SSQBBC for the equal voltage conversion ratio. The percentage ripple content in load voltage of HGBBC and TLBBC has been investigated, and a graph is drawn between percentage load voltage ripple vs duty cycle which is shown in Figure 17B. It appears that the load voltage of HGBBC has lesser ripple content as compared with TLBBC. Table 3 presents the overall comparison between the proposed HGBBC, TLBBC, and SSQBBC based on number of components that are used in the power circuits of the converters, voltage gain, and order of the converters. From Table 3, it appears that HGBBC and TLBBC have the same number of components in the power circuits. However, due to modification in the power circuit of the proposed HGBBC the overall performance has been improved as compared to TLBBC.

8 | CONCLUSION

An improved HGBBC with optimized Type III controller has been proposed and developed in this work. The proposed HGBBC has been implemented and results have been presented to validate the advantages of the developed converter over other two existing quadratic types of BBCs (TLBBC and SSQBBC). The proposed HGBBC produces high voltage gain with noninverting output voltage, which get rid of the limited voltage gain and negative output voltage problem that is associated in the conventional BBC. The overall voltage gain of HGBBC is the squared times the voltage gain of the conventional BBC and its source and load terminals are in the same polarity. The efficiency as well as overall performance in terms of dynamic response and percentage ripple content in load voltage of HGBBC has also been improved. It is seen that the proposed HGBBC exhibits better performance as compared with TLBBC and SSQBBC. A laboratory-scale experimental setup of closed loop HGBBC has been implemented and the simulated results are validated. The percentage efficiency of HGBBC, TLBBC, and SSQBBC has been measured by varying the duty cycle ratio, and it is found that HGBBC is more energy efficient than TLBBC and SSQBBC. The percentage ripple content in the load voltage of HGBBC and TLBBC has also been investigated and it is found that the load voltage of HGBBC has lesser ripple content as compared with TLBBC. The limitation of this converter is that its bandwidth is restricted due to having RHP zero in its small-signal model (ie, control-to-output transfer function).

The proposed HGBBC can be applied in DC-DC SMPC-based equipment which requires high voltage conversion efficiently either in step-up mode or in step-down mode. The proposed HGBBC can be applied in some real-time applications, such as electric cars, traction systems, solar vehicles, solar battery chargers, maximum power point tracking (MPPT) system, telecommunication power supplies, and defense equipment.

ORCID

Niraj Rana https://orcid.org/0000-0001-8561-3356

REFERENCES

1. Matsuo H, Harada K. The cascade connection of switching regulators. *IEEE Trans Indust Appl*. 1976;IA-12(2):192-198, Mar./Apr. https://doi.org/10.1109/TIA.1976.349401
2. Erickson RW, Maksimovic D. *Fundamentals of Power Electronics*. Berlin, Germany: Springer; 2007.
3. Mohammadzadeh Shahir F, Babaei E, Sabahi M, Laali S. A new DC-DC converter based on voltage lift technique. *Int Trans Electr Energy Syst*. 2016;26(6):1260-1286.
4. Banerjee S, Ghosh A, Padmanaban S. Modeling and analysis of complex dynamics for dSPACE controlled closed-loop DC-DC boost converter. *Int Trans Electr Energy Syst*. 2019;29(4):e2813. https://doi.org/10.1002/etep.2813
5. Ardi H, Ajami A, Sabahi M. Analysis and implementation of a novel three input DC-DC boost converter for sustainable energy applications. *Int Trans Electr Energy Syst*. 2019;29(4):e2801. https://doi.org/10.1002/etep.2801
6. Shen C-L, Chiu P-C. Buck-boost-flyback integrated converter with single switch to achieve high voltage gain for PV or fuel-cell applications. *IET Power Electron*. 2016;9(6):1228-1237.
7. Banaei MR, Bonab HAF. A novel structure for single-switch nonisolated transformerless buck-boost DC-DC converter. *IEEE Trans Ind Electron*. 2017;64(1):198-205.
8. Vinnikov D, Chub A, Kosenko R, Zakis J, Liivik E. Comparison of performance of phase-shift and asymmetrical pulse width modulation techniques for the novel galvanically isolated buck-boost DC-DC converter for photovoltaic applications. *IEEE J Emerg Sel Top Power Electron*. 2017;5(2):624-637.
9. Tsai C-H, Tsai Y-S, Liu H-C. A stable mode-transition technique for a digitally controlled non-inverting buck-boost DC-DC converter. *IEEE Trans Ind Electron*. 2015;62(1):475-483.
10. Wu H, Sun K, Chen L, Zhu L, Xing Y. High Step-up/step-down soft-switching bidirectional DC-DC converter with coupled-inductor and voltage matching control for energy storage systems. *IEEE Trans Ind Electron*. 2016;63(5):2892-2903.
11. Son H-S, Kim J-K, Lee J-B, Moon S-S, Park J-H, Lee S-H. A new buck-boost converter with low-voltage stress and reduced conducting components. *IEEE Trans Ind Electron*. 2017;64(9):7030-7038.
12. Rana N, Ghosh A, Banerjee S. Development of an Improved Tri-State Buck-Boost Converter with Optimized Type-3 Controller. *IEEE J Emerg Sel Top Power Electron*. 2018;6(1):400-415.
13. Ajami A, Ardi H, Farakhor A. Design, analysis and implementation of a buck-boost DC/DC converter. *IET Power Electron*. 2014;7(12):2902-2913.
14. Miao S, Wang F, Ma X. A new transformerless buck-boost converter with positive output voltage. *IEEE Trans Ind Electron*. 2016;63(5):2965-2975.
15. Zhang N, Zhang G, See KW, Zhang B. A single-switch quadratic buck-boost converter with continuous input port current and continuous output port current. *IEEE Trans Power Electron*. 2018;33(5):4157-4166.
16. Ding S, Wang F. A new negative output buck-boost converter with wide conversion ratio. *IEEE Trans Ind Electron*. 2017;64(12):9322-9333.
17. Banerjee S, Ghosh A, Rana N. 'Design and fabrication of closed loop two-phase interleaved boost converter with type-III controller', in *proc. 42nd Annual Conference of the IEEE Industrial Electronics Society (IECON 2016)*, 2016, pp. 3331-3336.
18. Cornea O, Andreescu G-D, Muntean N, Hulea D. Bidirectional power flow control in a DC microgrid through a switched-capacitor cell hybrid DC-DC converter. *IEEE Trans Ind Electron*. 2017;64(4):3012-3022.
19. Rana N, Kumar M, Ghosh A, Banerjee S. A novel interleaved tri-state boost converter with lower ripple and improved dynamic response. *IEEE Trans Ind Electron*. 2018;65(7):5456-5465.
20. Venable H D. 'The K-Factor: A new mathematical tool for stability analysis and synthesis', in *Proc. Powercon*, San Diego, 1983, pp. 1-10.
21. Hwu KI, Jiang WZ, Shieh J. 'Implementation of type III controller for KY converter based on PSIM', in *proc. 41st Annual Conference of the IEEE Industrial Electronics Society (IECON 2015)*, 2015, pp. 141-145.
22. Banerjee S, Ghosh A, Rana N. An improved interleaved boost converter with PSO based optimal type-III controller. *IEEE J Emerg Sel Top Power Electron*. 2017;5(1):323-337.
23. Foong HC, Tan MT, Zheng Y. 'An adaptive digital DC-DC converter based on particle swarm optimization', in *proc. 8th IEEE International Conference on Power Electronics (ECCE Asia)*, 2011, pp. 2805-2812.
24. Fermeiro JBL, Pombo JAN, Calado MRA, Mariano SJPS. A new controller for DC-DC converters based on particle swarm optimization. *Appl Soft Comput (Elsevier)*. 2017;52:418-434.

How to cite this article: Banerjee S, Rana N. Closed-loop control and performance analysis of a high-gain buck-boost converter with optimized type III controller. *Int Trans Electr Energ Syst*. 2019;e12158. https://doi.org/10.1002/2050-7038.12158